2020 IEEE/RSJ International Conference on Intelligent Robots and Systems (IROS)
October 25-29, 2020, Las Vegas, NV, USA (Virtual)

A Minimalistic Hyper-Flexible Manipulator: Modeling and Control

Amit Prigozin, *Student Member, IEEE* and Amir Degani, *Member, IEEE*

***Abstract* — Robotic manipulators can be found today in most industries, from autonomous warehouses to advanced assembly lines in factories. Most of these industrial robots are characterized by having non-flexible and highly rigid links. In dense and complex environments these manipulators require many degrees of freedom (DOFs) which complicates the mechanical structure of the manipulator, as well as the control and path planning algorithms. In this work we present a minimalistic approach to reduce the number of active DOFs by using non-rigid, Hyper-Flexible Manipulators (HFM). We introduce a dynamic model of the HFM as well as a control scheme to bring the end-effector to a desired position from known initial configuration. Finally, we present experiments that support the analytic part and simulative results of this paper.**

I. INTRODUCTION

In recent years, robots have been increasingly integrated into everyday life. The automation process simplifies work and increases productivity across various industries. In many cases, robots perform precise and repeatable tasks, such as placement of small components on a printed circuit board. These components can be minuscule, in the order of tenths of a millimeter. Due to the nature of such tasks, these robotic manipulators are characterized by non-flexible, highly rigid manipulators with zero backlash mechanisms. While there is no doubt that these properties are crucial to many tasks, in other situations, such properties only interfere with the successful completion of tasks. One of the classic examples is fruit harvesting; the complex structure of the branches may block the way to some of the fruit, while the rigid structure of the robot prevents it from circumventing the obstacles.

We hypothesize that in order to increase the efficacy of robotic manipulators in dense, complex environments, it is possible to use flexible manipulators. Most of the work done in the flexible manipulators field focuses on creating manipulators with many active degrees of freedom (DOFs), as it allows manipulating the arm between obstacles and towards the desired target. However, a new problem arises; the increase in DOFs dramatically increases the complexity of path planning algorithms as well as the control methods for such a manipulator, especially if all DOF are active, and where the uncertainty of configuration increases due to the flexibility of the links.

A. Prigozin is with the Civil and Environmental Engineering Department, Technion-Israel Institute of Technology, Haifa, Israel 32000 (e-mail: prigozin@campus.technion.ac.il).

A. Degani is with the Civil and Environmental Engineering Department and with the Technion's Autonomous Systems Program, Technion-Israel Institute of Technology, Haifa, Israel 32000 (corresponding author: e-mail: adegani@technion.ac.il).

The current work aims to show an alternative, minimalistic approach, to the presented problem; instead of using a high number of active DOFs, only a single active DOF at the base of the manipulator is controlled, while the rest of the structure is passive and flexible, unlike classic industrial rigid manipulators.

In order to simplify the governing equations, some of the simulations and experiments are performed on multi-link models. Fig. 1 shows an overlay of six snapshots of an experiment with an HFM model and the corresponding simulated trajectory. As seen, the Tool Center Point (TCP) moves along the calculated trajectory (marked in gray line). At the center of the structure, a DC motor, connected to the base of the Hyper-Flexible Manipulators (HFM), is the only active DOF. A reflective marker is located at the TCP, allowing data collection of the TCP position over time. As will be shown in later sections, using such a simple manipulator, with only a single actuator, allows coverage of 84% of the ideal workspace. In order to control the position of the TCP, a primary torque-control-loop has been implemented. This work will be the basis for future work, where the uncertainty of the TCP location can be decreased by using obstacles in the surroundings as pivot points, thus reducing the need for closed-loop control.

The paper is organized as follows: Sec. II reviews the related work and presents past progress in the field. Sec. III presents the modeling techniques which was chosen to be used for HFM. Sec. IV formulates how to control HFMs using only one active DOF in a way that allows coverage of most of the workspace. Sec. V describes the experimental setup used to verify the analytic and simulative results. We conclude with a discussion of the experiment results in Sec. VI.

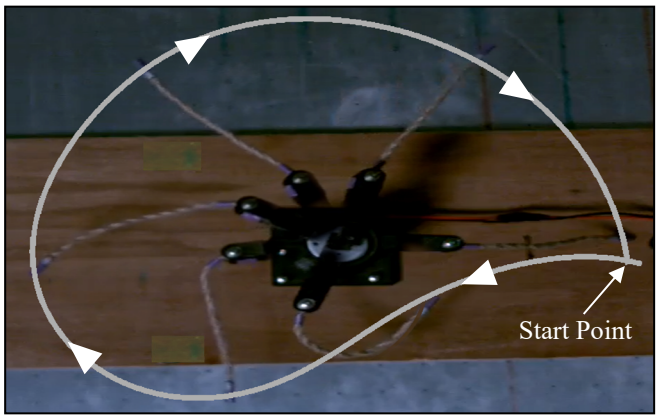

Figure 1. Overlaid snapshots from an experiment with an HFM. Beginning from the indicated "start point", the rotation direction is clockwise. The predicted trajectory of the TCP (i.e., the distal part of the flexible manipulator) taken from simulation is shown in gray with arrows marking the direction.

978-1-7281-6211-9/20/$31.00 ©2020 IEEE

II. Related Work

Deformable object manipulation is a relatively young field and has recently begun to gain momentum. Deformable objects are typically described using non-linear ordinary differential equation (ODE) and partial differential equation (PDE) systems. These are usually solved with finite-difference or finite-element techniques. Early endeavors in the field focused on modeling of hyper-flexible materials such as ropes, strings and chains. Previous studies can be classified by the type of modeling technique. These include two major approaches: PDE and multi-body.

In the PDE approach, the entire manipulator is described by a set of three equations for a planar manipulator or four equations for a spatial manipulator. One equation describes the force along the manipulator, and two (or three for spatial) equations describe the manipulator's position. Despite the low number of equations, they are coupled, non-linear, second-order partial differential equation, making them complicated to solve using numerical methods. It is important to note that all the projects that modeled HFM using the PDE approach used certain simplifications and assumptions, which led to the linearization of the model and a solution of a simple wave equation. To the best of our knowledge, no previous work solved the general PDEs for a planar or spatial HFM. As mentioned, the presented paper focuses on the general, non-linear case and therefore, the PDE method is irrelevant. One of the example of modeling deformable material as a PDE are Feng and Allen that evaluate of the effects of communication cables on underwater vehicles [1]

In the multi-link approach, there is a set of ODE equations, one for each link. As a result, the system can contain dozens or hundreds of equations, depending on the complexity of the model. Despite the large number of equations, the multi-link approach simplifies the governing equations as the equations are second-order, non-linear, ordinary differential equation, and therefore are quite simple to solve using basic ODE tools. Suzuki et al. performed a casting and winded task using hyper-flexible manipulators [2]–[4], Yamakawa et al. performed sonic-speed manipulations using an industrial robotic arm [5], and Winget et al. which studied submerged cables [6].

As the knowledge on HFM modeling increases, along with computational power, more researchers investigate techniques to control HFMs. There are two major control schemes for HFMs: non-prehensile and prehensile manipulation.

Non-prehensile manipulation is characterized by phases with no contact between the manipulator and the actuator, e.g., bouncing a ball. Mochiyama used a pneumatic system to cast the end-effector, which is connected by a flexible elastic rope to the ground, into the air [7]. In the work of Hatton et al., a manipulator cast a grasping tool into the air and wrapped it around a pole [8]. Fagiolini used a simple two-DOF robotic system to spin the end-effector at high velocity, and then released and cast it at a target [9].

In prehensile manipulation, constant contact is kept between the actuator and the HFM, as in our presented work. Examples of such works are Yamakawa et al., which used a serial industrial robotic arm to control a whip [10]–[13]. Suzuki used a simple one-DOF rotational robot to wrap a chain around a pole [3]. We aim to further investigate and analyze the minimalistic approach of using a single actuator to control HFMs.

Non-prehensile manipulation has its advantages, such as the ability to increase the workspace and reachable areas, which are inaccessible when using prehensile manipulation and using less active DOFs. The clear advantage of prehensile manipulation is the ability to change the control signal to the end-effector during manipulation. If, for example, there is a sudden disturbance, it is possible to sense and track the deviation of the end-effector and fix the actuation accordingly.

III. Modeling

In this work, the HFM is modeled using the multi-body approach. A set of N links are connected to each other by a revolute joint at the end of each link (as seen in Fig. 2). The angle, θ_i, of each link is defined with respect to the horizontal axis.

The model was developed using several assumptions: 1) the manipulator's structure is highly flexible but non-elastic (i.e., non-extendable as the case of a rope or cable); 2) the structure keeps a constant cross-sectional area and constant density; 3) the manipulator remains planar; 4) the mass of each link is concentrated at its center.

The equations of motion are written using the Lagrangian approach. The position of each end link is written as

$$\begin{cases} X_i = X_{i-1} + L \cdot \sin(\theta_i) \\ Y_i = Y_{i-1} - L \cdot \cos(\theta_i) \end{cases}. \quad (1)$$

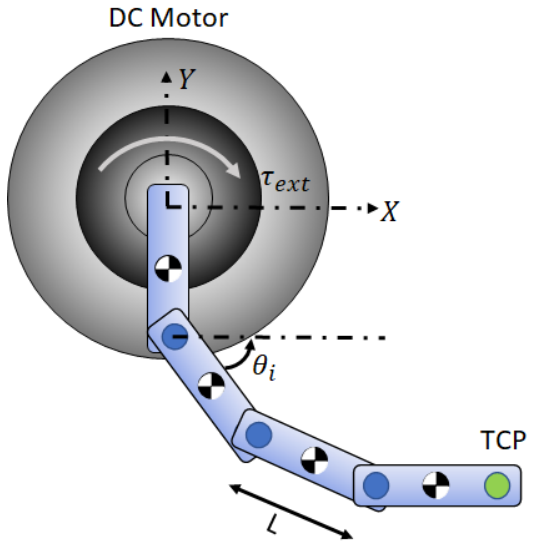

Figure 2. Schematic representation of a multi-link model of the HFM. The active DOF is the DC motor located at the center. Blue circles represent passive revolute joint, center of mass are shown at the center of each link, and the green circle represents the TCP position. Positive torque, τ_{ext}, is in the clockwise direction.

The initial condition for the position is set to zero, i.e., $x_0 = 0, y_0 = 0$ and the position of each link is defined as $P_i = [x_i \quad y_i]$. The position vector is now derived to define the velocity vector

$$V_i = \frac{dP_i}{dt} \tag{4}$$

which is then used to find the total kinematic energy of the system

$$T = \sum(\tfrac{1}{2} m V_i V_i^T), \tag{5}$$

where, m represents the link's mass. Since the manipulator operates in a planar workspace perpendicular to gravity, the potential energy in the system is constant and can be neglected.

Finally, the non-preserving forces, which are due to friction in the joints, are defined as

$$D = \frac{1}{2} b \left(\dot{\theta}_1^2 + \sum_{i=2}^{N} \left(\dot{\theta}_i - \dot{\theta}_{i-1} \right)^2 \right), \tag{6}$$

where, b is the dissipation constant.

The Lagrangian is

$$\frac{d}{dt}\left(\frac{\partial T}{\partial \dot{q}}\right) - \frac{\partial T}{\partial q} + \frac{dD}{d\dot{q}} = \tau_{ext}, \tag{7}$$

where, τ_{ext} is the external forces vector and q is the manipulator's configuration. The result is a set of N ODE equations.

IV. Control Scheme

After obtaining the equations of motion, the next step is to control the system in such a way that the controller can bring the TCP to a desired position. At first, a series of simulations were conducted with a constant applied torque to the base link. All simulations started with the same initial horizontal conditions: $\theta_i = 0, \forall i$ and $\dot{\theta}_i = 0, \forall i$. In all simulations, only the first cycle of the trajectory of the HFM was analyzed. Fig. 3 depicts trajectories using four different torque inputs.

As can be seen in Fig. 3, as the applied torque is changed, so does the trajectory of the TCP within the plane. An important result of the simulations is that the trajectories are non-intersecting. As a result, for each point in the space, there is only one trajectory that passes through that point. Fig. 4 depicts the full workspace for a range of torques. Each line represents a different input torque. Fig. 4a depicts the workspace for the initial condition $\theta_i = 0, \forall i$, for both positive and negative input torques. Fig. 4b depicts the workspace for the initial conditions $\theta_i = 0$ as well as $\theta_i = \pi, \forall i$. Fig. 4c shows the workspace for the initial conditions $\theta_i = 0, \theta_i = \pi/2,\ \theta_i = 3\pi/4,$ and $\theta_i = \pi/2, \forall i$. Due to symmetry considerations, the system's dynamic behavior does not change because of different initial conditions. In the last case (Fig. 4c), the active workspace of the HFM is approximately 84% from the entire theoretical workspace of the manipulator, as calculated from Fig. 4.

At this point, for any given desired point, the desired input torque can be calculated in such a way that the TCP will pass through the point. However, in real-world situations, disturbances occur, as well as variances in the manipulator's parameters. In order to reach the desired point with the required precision, a closed control loop can be used. The motivation for our control scheme is that all trajectories

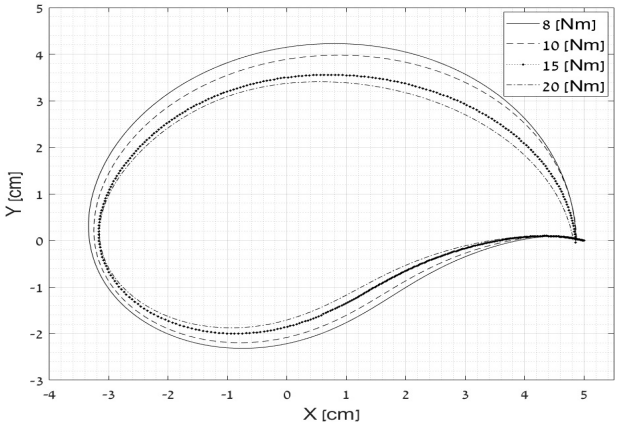

Figure 3. TCP trajectory for four different input torques. As can be seen, all the trajectories share the same basic nominal trajectory shape and do not

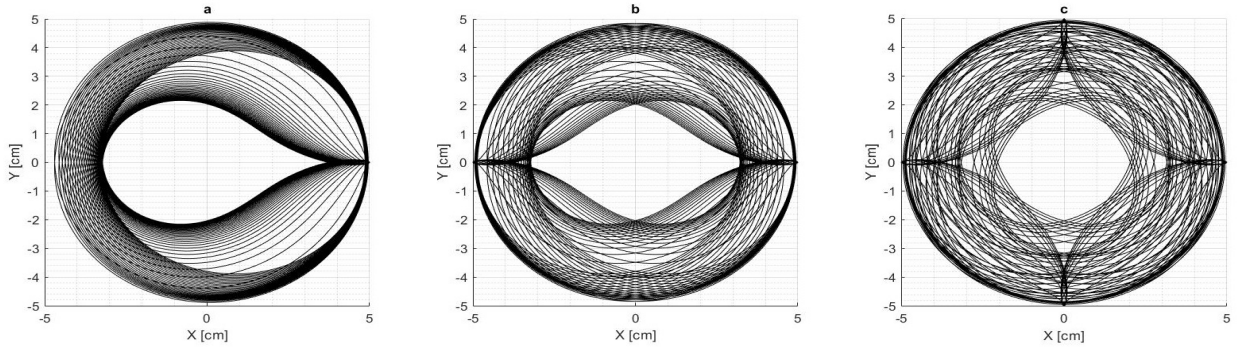

Figure 4. The effective workspace of the manipulator depending on the initial conditions from simulations. In all the figures the torque range between [-0.3:0.3] Nm. a) the manipulator starts from one starting point in all tests ($\theta_i = 0°$). b) the manipulator starts from two different starting points ($\theta_i = 0°, 180°$). c) the manipulator starts from four different strating points ($\theta_i = 0°, 90°, 180°, 270°$).

(seen in Fig. 3) have the same nominal shape, with mostly scale differences. We can refer to this general trajectory shape as the nominal trajectory. In order to move between trajectories, a short torque impulse is applied to the base link. As a result, the TCP changes its trajectory while keeping the nominal trajectory shape. A simple PID controller was used in order to control the torque impulses. The error for the PID controller was defined as the radial difference in polar coordinates. The use of a closed loop control increases the robustness to external perturbations in the environment and variance in the HFM parameters.

V. Experimental Setup

The experimental system consists of a sensing system and the active HFM manipulator. The sensing system includes a motion tracking system with six Vicon™ T-10s cameras, located above the experimental setup, providing a 1000 Hz frame rate at 1120×896 pixel resolution. Additionally, a Phantom™ Miro LAB-320 high-speed camera records at 3500 Hz frame rate and 1024×768 resolution.

The Vicon™ cameras are used to capture the TCP trajectory of the HFM, mostly for real-time control. On the other hand, the Phantom™ camera is used to gain better understanding of the dynamic behavior of the HFM, and simplified system analysis, by allowing us to view the manipulation action again in slow-motion.

The manipulator consists of a DC motor which acts as the single active DOF in the system. The motor is connected in a direct-drive configuration to either the HFM (e.g., rope) or to the simplified HFM, as can be seen in Fig. 5. The motor is controlled by an H-Bridge connected to an Arduino DUE microcontroller. A serial, wired, communication between the microcontroller and a dedicated Matlab™ computer, which in turn is connected to the Vicon™ system, allows to control the desired torque at any moment. This allows working in either open-loop or closed-loop. Four reflective markers for use of the Vicon™ system are located: one at the end of the manipulator to record the TCP trajectory, and three on the base plate as reference points. The experimental setup can be seen in Fig. 5.

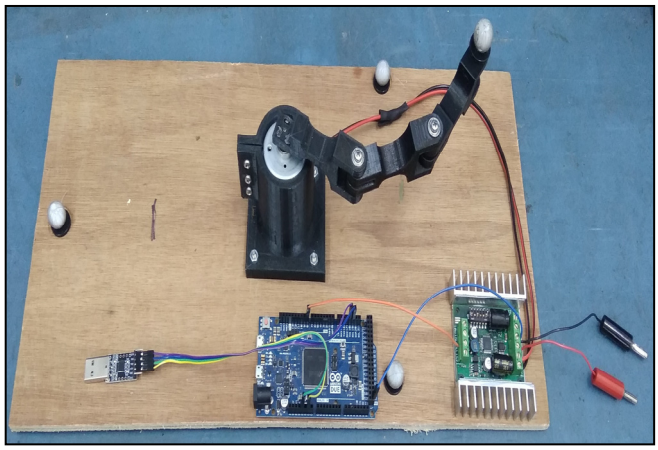

Figure 5. Experimental setup – including the DC motor, connected to the simplified HFM model, H-bridge, and microcontroller.

VI. Results

The final stage was to validate the analytic model, simulations, and the control scheme with a set of experiments. A simplified multi-link setup was built, as described in Fig. 5. The length of each link is L=0.06 m, and the mass is m=0.013 kg. To estimate the dissipation factor of the manipulator, a set of experiments were performed, and a range of 11 - 18 kg·m/s was deduced. The dissipation factor is a function of the velocity due to non-linear behavior in the revolute joints. The experiments include applying known torques into the system, recording the TCP trajectory and performing curve fitting with simulations results. The dissipation factor represents the energy loss in the system due to friction in the joints.

With all the parameters of the manipulator verified, we tested if the manipulator is able to reach desired points in its workspace, as previously described. A set of experiments were conducted under different constant input torques. Fig. 6 shows the results in the polar, $r-\theta$, plane. In the following setup, the input torques were in the range of 0.02 to 0.09 Nm. As can be seen, in the effective workspace of the manipulator, i.e. between 0° to 180°, the TCP can reach nearly every desired point between the radius of 6 cm to 16 cm. It is important to remember that in the setup, the manipulator was only rotating clockwise, using only positive torques, while being able to rotate clockwise and anticlockwise and by that reaching desired points in the right-half plane (as seen in Fig. 7). The effective workspace in Fig. 7 is approximately 61.9% of the total workspace. As mentioned in Sec. IV, by changing the initial condition of the position, the effective workspace of the manipulator can be increased to up to 84%.

Fig. 6 also shows the uncertainty of the TCP trajectory. The shaded area around each graph represents the variance of the TCP position along the trajectory. The results are based on a set of 50 experiments with the same initial conditions and the same control input. The maximum variance was about 0.93 cm, 6.11% of the total manipulator length. As can be anticipated, the highest uncertainty was at the first half of the motion. After the manipulator reaches about 180°, the centrifugal force helps reduce the uncertainty in the system and hence the lower variances. The mean-variance along the complete motion was 0.2978 cm.

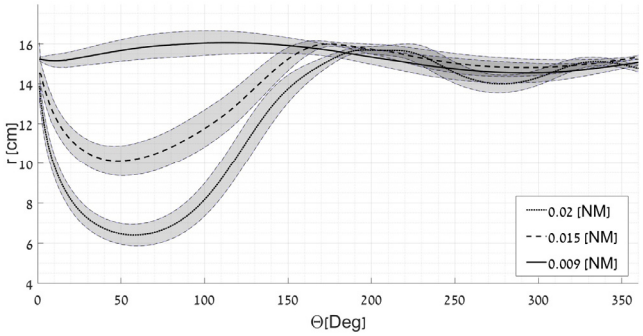

Figure 6. The actual workspace from a set of experiments. The graph is presented in the $r-\theta$ space. On each graph, the variance of the position based on 50 experiments is shown in grey shade.

Next, we use our control scheme to control the manipulator, as suggested in Sec. IV. Fig. 8 shows the results of such simulations. The simulation includes uncertainty in the HFM parameters (mass and dissipation factor) of up to 5%. Furthermore, random noise of 2% was added to both the control input and the measured data. As seen in the figure, the control loop manages to close the loop after about 130° using only the simple PID controller. Based on trial and error, the proportional gain was set to 1, and the integrator gain was set to 0.1. The controller output is added to the initial constant torque that we calculated previously. These results are promising, as even the simple controller used in this case achieved satisfactory results. In the following simulation, the control loop operates at 250 Hz.

As mentioned above, the research goal is to model and control an HFM, but up to now, only multi-link manipulators were analyzed and tested. In the next set of experiments, the multi-link manipulator was replaced with different types of flexible ropes. Figs. 10 and 11, show experiments with ropes of different diameters: 10 mm and 4 mm, respectively. As can be seen, the nominal trajectory of the ropes in Fig. 9 is similar to the nominal trajectory seen in the simulations of the multi-link model (Fig. 4). The similarity in the dynamic model of the multi-link and the HFM allow us to use similar control techniques on both, as at the limit of $N \to \infty$ we arrive at the same physical model. By that, the controller can bring the TCP of the rope to any desired point in our workspace. It is important to note that, in order to reduce computation time, all experiments were compared to a multi-link simulation with three links, and therefore some of the trajectories did not have a perfect fit. It is possible to increase the number of links and increase the accuracy of the model, however, even with three links, the fit between the HFM and the multi-link simulation is sufficient. Although the two ropes share similar properties, there are still differences between their trajectories. These differences result mostly from different dissipation factors of the two ropes, as the thin rope has lower dissipation factor compared to the other. The low dissipation factor of the thin rope leads to a slightly different dynamic behavior, and therefore a slight change in the TCP trajectory. However, as can be seen, both ropes still track the nominal trajectory quiet well.

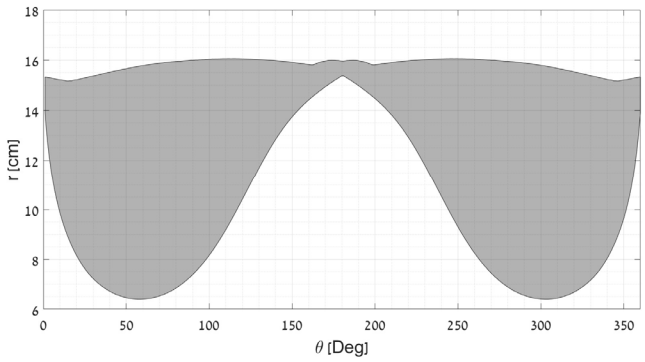

Figure 7. Experimenal results of the effective workspace in r-θ space of the multi-body manipulator with three links.

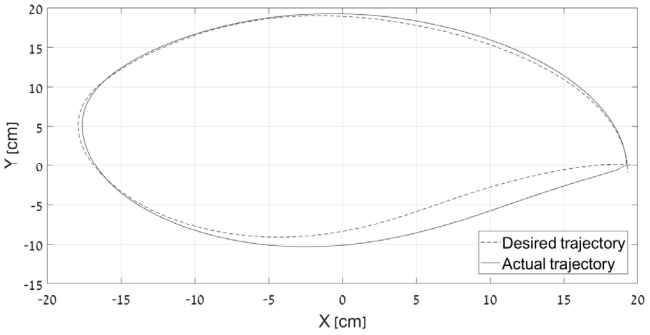

Figure 8. Simulation of controlling the trajectory in closed-loop. The continuous line is the actual trajectory while the dotted line is the desired trajectory. The initial condition in the current figure is (20,0) and the manipulator is rotating clockwise.

Finally, a set of "grasping" experiments were performed with the multi-link simplified model. Fig. 10 and Fig. 11 show snapshots of a simple grasping experiment at various desired target locations. In both experiments, the manipulator grasps an object using a two-sided tape. In the experiments, the target was placed at different desired locations and the control input was set accordingly to the simulations results. In both experiments, the manipulator collects the target successfully. The supplementary video demonstrates both the basic manipulations with HFMs and the grasping experiments. Fig. 1 shows snapshots of an experiment with using a flexible rope with simulation results overlaid on top. The fit between the experiments and the simulation reinforce the model's validity.

VII. Conclusions and Future Work

The presented paper introduced a new manipulation approach that can be useful for dense, complex environments. A minimalistic hyper-flexible robotic arm with a single actuator can be used in such environments. The paper presented a modeling technique for HFMs based on the Lagrangian approach. After deriving the full dynamic equations of motion, an approach was introduced for controlling the HFM using torque control in both open and closed-loop. The actual workspace of the manipulator was analyzed and compared to the theoretical one. Moreover, the

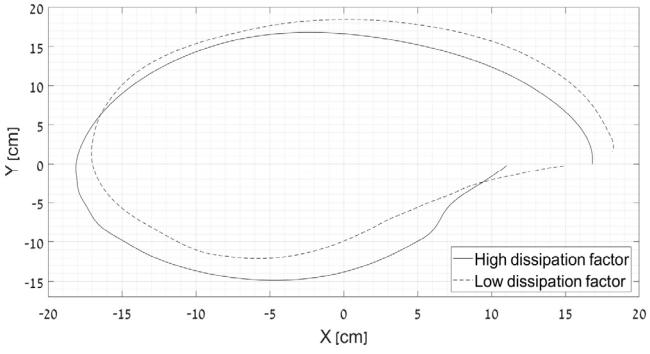

Figure 9. Experimental results with HFMs (Rope) with low and high dissipation factors. The graph depicts the TCP trajectory in space.

variances of the trajectories were demonstrated. As discussed in Sec. VI, a variance of less than 6.11%, is adequate for most tasks. A comparison between the multi-link and actual HFM (i.e., rope) was then conducted for serval rope diameter. Finally, a simple demonstration of grasping using the HFM, was performed.

In future endeavors, the work will be extended to reduce the need for a close-loop control by leveraging obstacles in the environment to decrease the uncertainty of the manipulator's position. We envision that by allowing the center part of the HFM to collide with the environment, the workspace can be increased, while reducing uncertainty. Furthermore, future work will include work with hyper-flexible elastic manipulators which can also elongate to increase the workspace and achieve more complex trajectories.

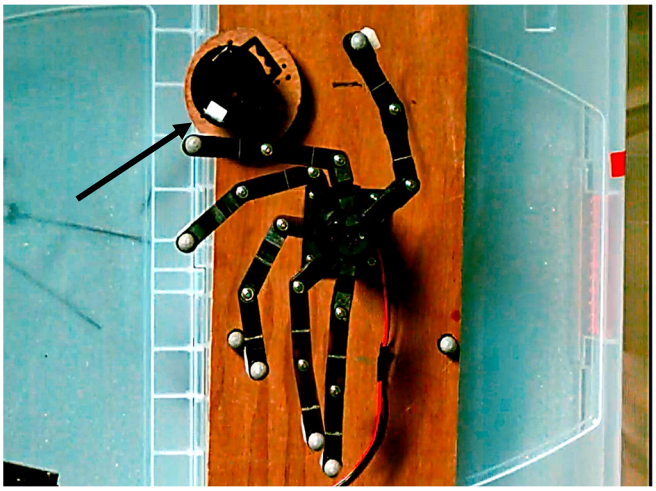

Figure 10. Overlaid snapshots of a simple grasping experiment. In the following experiment the target was placed in the outer area of the workspace. Black arrow indicates the target position before grasping. Red arrow marks the target after grasping.

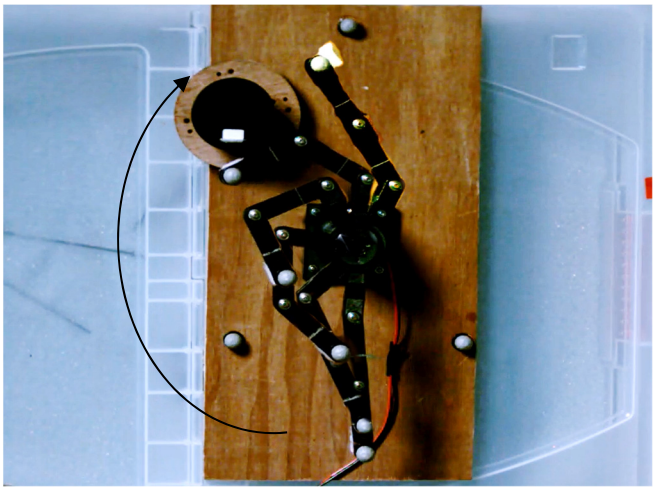

Figure 11. Overlaid snapshots of a simple grasping experiment. In the following experiment the target was placed in the inner area of the workspace.

REFERENCES

[1] Z. Feng and R. Allen, "Evaluation of the effects of the communication cable on the dynamics of an underwater flight vehicle," *Ocean Eng.*, vol. 31, no. 8–9, pp. 1019–1035, 2004.

[2] T. Suzuki, Y. Ebihara, and T. Suzuki, "Casting Control for Hyper-Flexible Manipulation," *Proc. 2007 IEEE Int. Conf. Robot. Autom.*, pp. 10–14, 2007.

[3] T. Suzuki, Y. Ebihara, Y. Ando, and M. Mizukawa, "Casting and winding manipulation with hyper-flexible manipulator," *Proc. IEEE Int. Conf. Intell. Robot. Syst.*, pp. 1674–1679, 2006.

[4] T. Suzuki, Y. Ebihara, and K. Shintani, "Dynamic analysis of casting and winding with hyper-flexible manipulator," *Proc. Int. Conf. Adv. Robot.*, vol. 2005, pp. 64–69, 2005.

[5] Y. Yamakawa, K. Odani, and M. Ishikawa, "Sonic-speed manipulation of a bull whip using a robot manipulator," *Proc. IEEE/ASME Int. Conf. Adv. Intell. Mechatronics, AIM*, vol. 2016-Septe, pp. 1139–1144, 2016.

[6] J. M. Winget and R. L. Huston, "Cable dynamics-a finite segment approach," *Comput. Struct.*, vol. 6, no. 6, pp. 475–480, Dec. 1975.

[7] H. Mochiyama, H. Nakajima, and T. Hatakeyama, "Chameleon-like Shooting Manipulator for Accurate 10-meter Reaching," *10th Asian Control Conf.*, 2015.

[8] L. Hill, T. Woodward, H. Arisumi, and R. L. Hatton, "Wrapping a target with a tethered projectile," *Proc. IEEE Int. Conf. Robot. Autom.*, pp. 1442–1447, 2015.

[9] A. Fagiolini, F. A. W. Belo, M. G. Catalano, F. Bonomo, S. Alicino, and A. Bicchi, "Design and control of a novel 3D casting manipulator," *Proc. IEEE Int. Conf. Robot. Autom.*, pp. 4169–4174, 2010.

[10] Y. Yamakawa, K. Odani, and M. Ishikawa, "Sonic-speed manipulation of a bull whip using a robot manipulator," *Proc. IEEE International Conference on Advanced Intelligent Mechatronics (AIM)*, 2016, pp. 1139–1144, 2016.

[11] K. Ito, Y. Yamakawa, and M. Ishikawa, "Winding manipulator based on high-speed visual feedback control," *Proc. IEEE Conf. Control Technol. Appl. CCTA 2017*, pp. 474–480, 2017.

[12] Y. Yamakawa, A. Namiki, and M. Ishikawa, "Dexterous manipulation of a rhythmic gymnastics ribbon with constant, high-speed motion of a high-speed manipulator," *Proc. IEEE Int. Conf. Robot. Autom.*, pp. 1896–1901, 2013.

[13] Y. Yamakawa, A. Namiki, and M. Ishikawa, "Motion planning for dynamic knotting of a flexible rope with a high-speed robot arm," *Proc. IEEE/RSJ 2010 Int. Conf. Intell. Robot. Syst.*, pp. 49–54, 2010.